Disorder-based Design Screening of a Semitransparent Ternary Organic/Silicon Four-Terminal Tandem Solar Cell

Mina Piralaee[1,2]

[1]*Faculty of Physics, University of Tabriz, Tabriz 51665-163, Iran.*

[2]*Photonics Devices Research Group, Research Institute of Applied Physics and Astronomy, University of Tabriz, Tabriz 51665-163, Iran*

Received: 2026-07-16 Final revised: 2026-8-16 Accepted: 2026-9-10

Abstract

Ternary organic solar cells provide greater flexibility in controlling light absorption, molecular packing, phase separation, and charge transport. In this work, a MATLAB-based model is used to investigate a semitransparent D18:L8-BO organic top cell optically coupled to crystalline silicon in a four-terminal (4T) tandem configuration. The effects of NVN concentration (0–20%) and Ag rear-electrode thickness (3–15 nm) are evaluated over a defined parameter range. The highest calculated output is obtained at 20% NVN and an Ag thickness of 3 nm. Under these conditions, the top-cell power-conversion efficiency (PCE) reaches 17.95%, while the normalized silicon power contribution is 16.58%, giving a total 4T PCE of 34.53%. The average visible transmittance (AVT) is 67.16%, and the silicon short-circuit current density is 28.08 mA cm^{-2}. The corresponding light-utilization efficiency (LUE) and figure of merit (FOM) are 12.05 and 23.19, respectively. These results provide a comparative basis for design screening rather than a prediction of fabricated-device performance. Experimental validation using a matching semitransparent device is still required.

Keywords: ternary organic solar cell; semitransparent photovoltaics; static and dynamic disorder; average visible transmittance; light-utilization efficiency; four-terminal tandem; crystalline silicon.

1. Introduction

Ternary organic solar cells (OSCs) provide an additional degree of freedom for tuning light absorption, molecular packing, phase separation, and charge transport [1-4]. By selecting an appropriate third component, researchers can alter the active-layer morphology and electronic properties beyond what is possible in a binary blend. The resulting changes are material- and processing-dependent, so the benefits of ternary blending must be evaluated for each specific system. The D18:L8-BO:NVN blend is relevant to this study because a recent experimental report associated NVN incorporation with reduced static and dynamic disorder, improved molecular packing and morphology, higher photoluminescence quantum yield (PLQY), and lower non-radiative energy loss [1]. That study reported a PCE of 20.80% for an optimized opaque ternary device [1]. This value is used here only as background context because an opaque cell and the semitransparent top cell considered in the present design have different optical requirements and device structures. For semitransparent OSCs, PCE alone is insufficient as a design criterion: electrical output must be considered alongside visible-light transmission [5, 6]. Average visible transmittance (AVT) quantifies the visible transmission of a device, while light-utilization efficiency (LUE) combines electrical output with AVT under a specified definition [6, 7]. These metrics are useful for comparing candidate designs, but their interpretation depends on the wavelength range, weighting function, and precise definition adopted.

Semitransparent OSCs are being explored for applications such as building-integrated photovoltaics and smart windows, where power generation must coexist with partial transmission of incident light [5, 8]. In a four-terminal (4T) tandem, light transmitted through the top cell can be absorbed by the silicon bottom cell. Because the sub cells operate electrically independently, the current-matching constraint associated with a two-terminal tandem is avoided [9].

High-performance D18-based OSCs, semitransparent devices employing ultrathin metallic electrodes, and organic/silicon 4T tandems have each been investigated previously [6, 7, 9-13]. The present study does not introduce a new material, report a fabricated device, or claim a validated predictive model. Its contribution is a transparent, parameterized screening workflow that varies NVN concentration and ultrathin Ag thickness together, estimates the top-cell response and the silicon contribution from transmitted light, and reports electrical and transparency-related metrics on a common incident-power basis. Reference [13] addresses a MoO_3/Ag/MoO_3 transparent-electrode strategy, whereas [9] evaluates selected 4T tandem configurations. Neither study is treated as experimental validation of the specific D18:L8-BO: NVN stack considered here. The advance claimed here is therefore the integrated comparison procedure and explicit accounting of assumptions, rather than a new experimentally established mechanism.

2 .Theory and Methodology

2.1. Device Structure and Energy-Level Alignment

The proposed architecture consists of a semitransparent ternary organic top cell optically coupled to a crystalline-silicon bottom cell. The top-cell active layer is D18:L8-BO: NVN and the rear electrode is ultrathin Ag. Transparent electrodes and ultrathin metal layers are commonly investigated for semitransparent organic photovoltaics

because they balance electrical collection against optical transmission [6, 8]. The proposed layer arrangement and energy-level alignment are illustrated in Figure 1.

The modeled top-cell stack is glass/ITO/ZnO/D18:L8-BO: NVN/HTL/Ag. ITO is the transparent electrode, ZnO is the electron-transport layer (ETL), and D18:L8-BO: NVN is the photoactive layer. The HTL/Ag layers provide hole extraction and form the semitransparent rear contact. The bottom cell is represented as a crystalline-silicon absorber with a rear metal contact. Because the two sub cells are electrically independent in the 4T configuration, their power contributions are calculated separately and then added after normalization to the same incident irradiance.

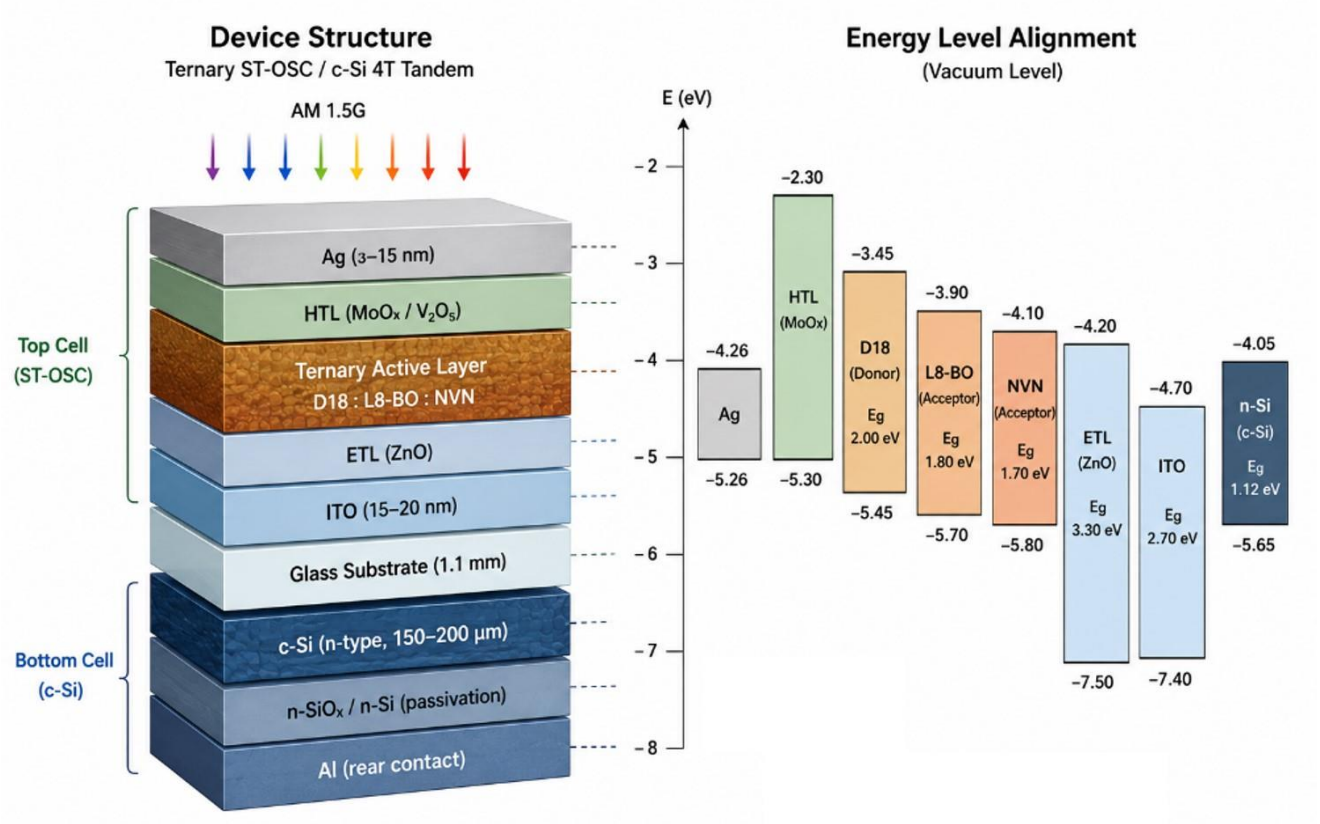


Fig. 1. Schematic of the proposed semitransparent ternary organic solar cell/crystalline-silicon four-terminal tandem and its energy-level alignment.

2.2. Optical and Electrical Modeling

The two swept design variables are NVN concentration (0–20%, in 0.5-percentage-point increments) and Ag thickness (3–15 nm, in 0.5 nm increments). The wavelength grid covers 300–1100 nm at 2 nm intervals, and the incident irradiance is normalized to 1000 W m^{-2} (100 mW cm^{-2}). The MATLAB implementation uses prescribed spectral and electrical functions. It does not use measured n(λ) and k(λ) data for the complete layer stack, an optical fit to measured spectra, or an experimentally calibrated diode model. The reported values are consequently conditional on the model assumptions and should be interpreted as design-screening estimates, not predictions of device performance. The power conversion efficiency is calculated using Equation1 as below.

$$PCE = \frac{J_{SC} \times V_{OC} \times FF}{P_{in}} \times 100 \quad (1)$$

Where J_{SC}, V_{OC}, FF are the short current density, open-circuit voltage and fill-factor respectively. The J_{SC} is estimated by integrating the transmitted photon flux weighted by an assumed effective silicon external quantum efficiency (EQE) as represented in Equation2. Neither this effective EQE nor the top-cell spectral functions represent a measured spectrum for the proposed stack. The silicon power contribution is estimated using the calculated $J_{sc,Si}$ together with fixed assumed values of $V_{oc,Si} = 0.72$ V and $FF_{Si} = 0.82$.

$$J_{sc,Si} = q\int \phi_{AM_{1.5}}(\lambda) T_{top}(\lambda) EQE_{Si}(\lambda) d\lambda \quad (2)$$

The total 4T PCE is obtained by adding the top-cell PCE and the silicon power contribution, each normalized to the same incident irradiance as represented in Equation.3. while, LUE is defined here as PCE_{top}(%) × AVT (fraction), and FOM as PCE_{4T} (%) × AVT (fraction). These are dimensionless comparative indices under the definitions used in this study.

$$PCE_4T = PCE_{top} + PCE_{si} \quad (3)$$

In Equation.3, the silicon contribution is normalized to the same incident irradiance used for the top cell, rather than to the reduced optical power reaching the silicon cell.

2.3. Disorder Modeling

Static and dynamic disorder are represented by separate concentration-dependent phenomenological descriptors. They are not direct measurements of energetic-disorder distributions and have not been calibrated against experimental data for the proposed semitransparent stack. Their qualitative form is motivated by the experimental report on the opaque D18:L8-BO:NVN system [1] and by work distinguishing static from dynamic disorder [14]. Thus, the direction of the trends is a literature-informed modeling assumption; the numerical magnitudes are prescribed rather than experimentally determined. The NVN concentration, C_{NVN}, denotes the numerical percentage of NVN in the ternary active layer and is varied from 0 to 20. The normalized static- and dynamic-disorder descriptors are defined by Eqs. (4a) and (4b), respectively.

$$D_s = 1 - 0.55[1 - \exp(-C_{NVN}/5)] \quad (4a)$$

$$D_d = 1 - 0.70[1 - \exp(-C_{NVN}/4)] \quad (4b)$$

The coefficients 0.55 and 0.70 and the characteristic concentration parameters 5 and 4 are phenomenological choices that impose saturating decreases in the two descriptors. They are not fitted parameters, measured constants, or statistical confidence limits. The mobility factor in Eq. (5) is also prescribed.

$$\mu_{rel} = 1 + 0.35[1 - \exp(-C_{NVN}/5)] \quad (5)$$

Here, μ_{rel} denotes the relative mobility factor. The prescribed function represents a saturating increase in effective mobility with increasing NVN concentration.

3. Results and Discussion

Table 1 summarizes the selected configuration and its modeled performance. Within the tested grid, the highest calculated 4T PCE occurs at 20% NVN and 3 nm Ag. This point lies at the upper boundary of the NVN range and the lower boundary of the Ag

range. It is therefore the best-performing point within the parameter space examined, not evidence of a global optimum outside those limits.

Table 1. Model-derived performance metrics at the highest-output point within the investigated parameter grid.

Parameter	Optimized value
NVN concentration	20%
Ag thickness	3 nm
Top-cell PCE	17.95%
Silicon power contribution (incident-power normalized)	16.58%
4T PCE	34.53%
AVT	67.16%
LUE = PCEtop × AVT fraction	12.05
FOM = PCE4T × AVT fraction	23.19
Jsc,Si	28.08 mA cm^{-2}

Figure 2 shows the calculated 4T PCE across the NVN–Ag parameter grid. The maximum occurs at 20% NVN and 3 nm Ag, on the boundary of the tested ranges.

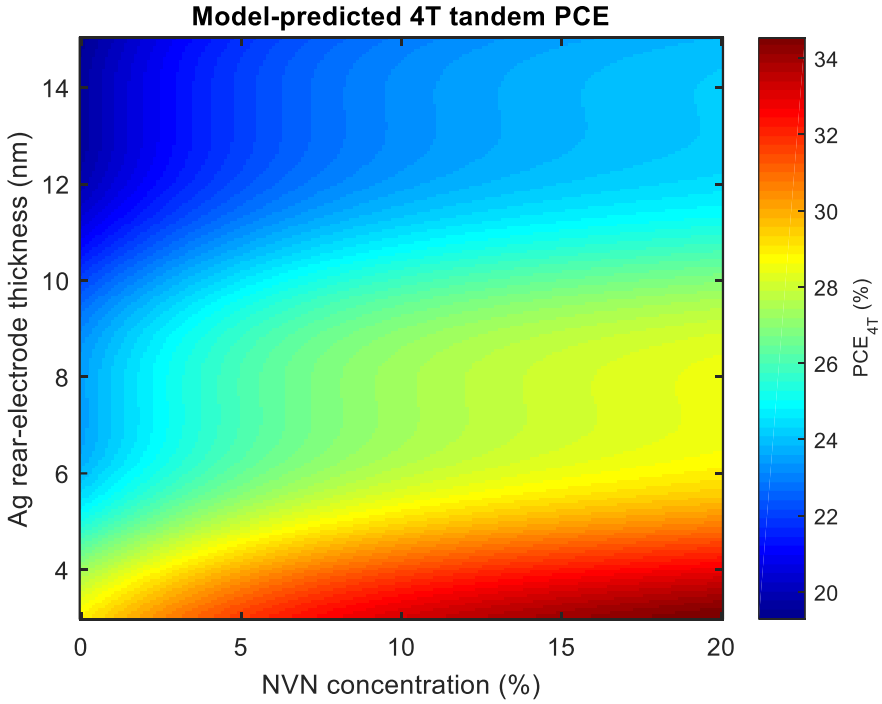


Fig. 2. Model-estimated 4T tandem PCE as a function of NVN concentration and Ag thickness. The axes show NVN concentration (%) and Ag thickness (nm); the color bar reports PCE_4T (%).

In this parameterized model, changing Ag thickness changes the assumed spectral transmission and, consequently, the photon flux available to the silicon cell. At the

selected point, the calculated AVT is 67.16% and $J_{sc,Si}$ is 28.08 mA cm^{-2}. Figure 3 shows the model-generated transmission, reflection, and total absorptance spectra used in estimating the silicon photocurrent.

The spectrum is generated from the parameterized functions described in Section 2; it is not calculated from measured optical constants for the full stack. It illustrates how the model partitions incident light into transmission, reflection, and absorption. The absolute spectral values require validation against measured optical data. Figure 4 shows the normalized static- and dynamic-disorder descriptors.

At the selected configuration, the model gives $J_{sc,top} = 26.23$ mA cm^{-2}, $V_{oc,top} = 0.8713$ V, $FF_{top} = 0.7982$, and an optical/electrode multiplier of 0.9839, yielding a top-cell PCE of 17.95%. With the same optical/electrode multiplier but without the prescribed disorder-dependent electrical corrections, the reference-model PCE is 15.90%. Relative to the published 20.80% opaque-cell benchmark, the modeled top-cell value is lower by 2.85 percentage points, equivalent to 13.7% of the benchmark value. This comparison is not like-for-like because the device architecture and transparency target differ.

Figure 5 compares the reference and disorder-informed model outputs with the 20.80% opaque-device result for context. The difference between the two model states quantifies sensitivity to the imposed disorder-related corrections only; it is not a validation of those corrections.

Taken together, the results show how the current parameterized model can rank candidate configurations when the same assumptions are applied consistently.

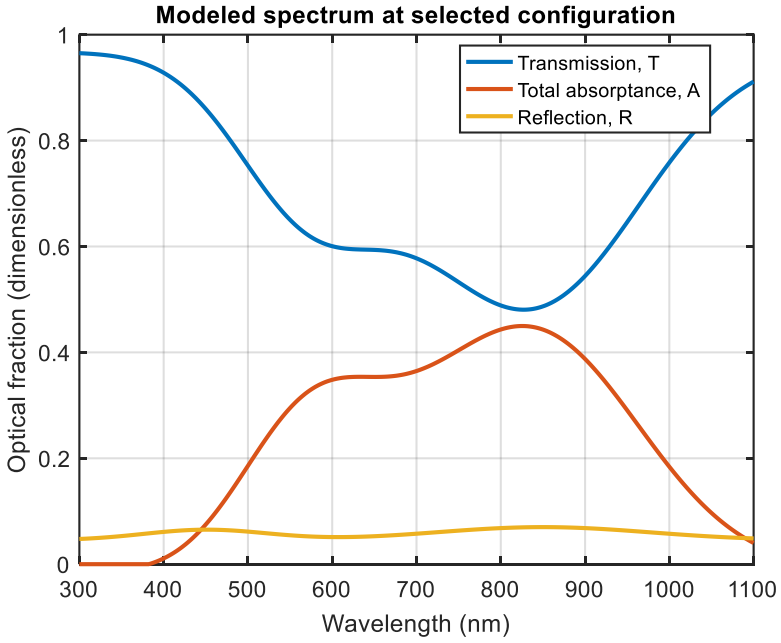


Fig. 3. Spectral transmission, reflection, and total absorptance at 20% NVN and 3 nm Ag.

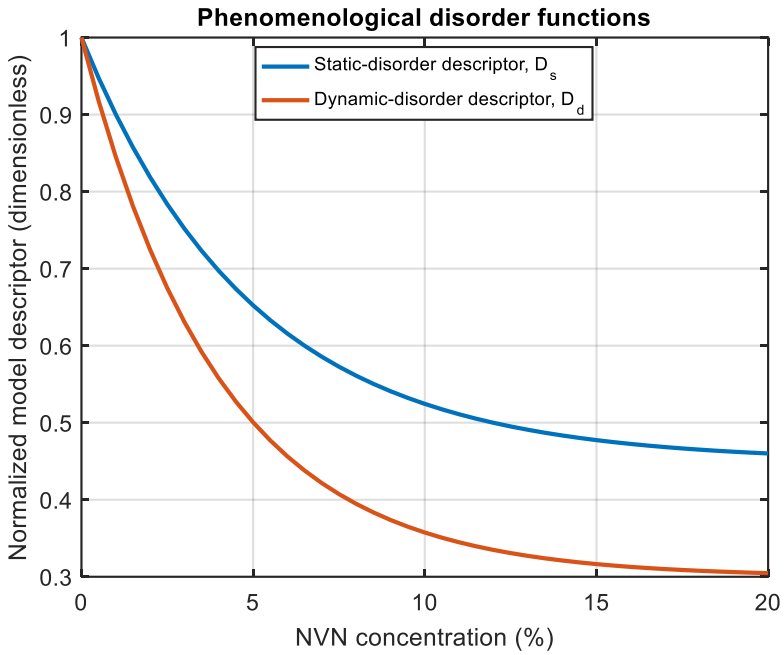


Fig. 4. The normalized static- and dynamic-disorder descriptors as functions of NVN concentration.

5. Conclusion

This study presents a MATLAB framework for screening a semitransparent D18:L8-BO: NVN/crystalline-silicon 4T tandem over NVN concentrations of 0–20% and Ag thicknesses of 3–15 nm. Within the tested grid, the highest modeled 4T PCE is 34.53% at 20% NVN and 3 nm Ag, with AVT = 67.16%. At this point, the modeled top-cell PCE is 17.95%, the silicon contribution normalized to the incident irradiance is 16.58%, and $J_{sc,Si}$ is 28.08 mA cm^{-2}; LUE and FOM are 12.05 and 23.19 respectively. The optical inputs and disorder functions are phenomenological and have not been calibrated against a measured semitransparent device. The results should be used to compare candidate designs under stated assumptions, not as validated predictions of device efficiency. Experimental validation with a matched semitransparent D18:L8-BO: NVN device is a necessary next step.

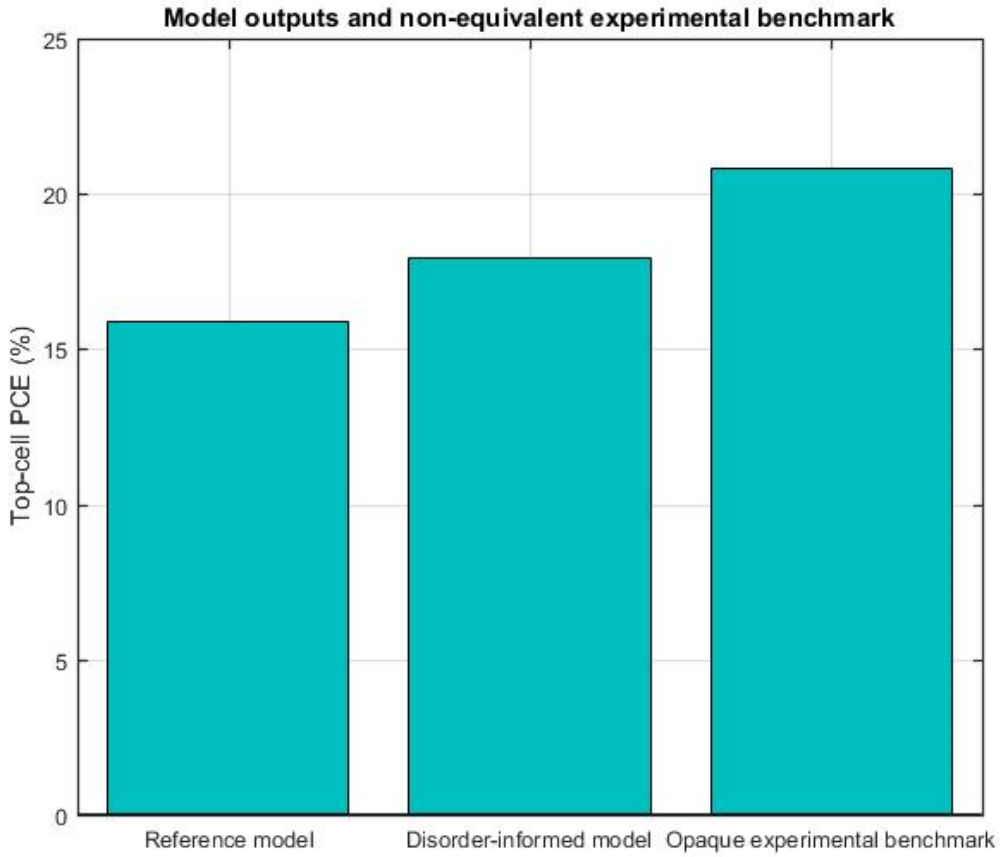


Fig. 5. Top-cell PCE from the reference and disorder-informed model states, alongside the published 20.80% opaque-device benchmark [1].

6. Declarations Conflict of Interest:

The author declares no conflict of interest.

Data Availability: The MATLAB code and master numerical dataset supporting this study can be provided by the corresponding author upon reasonable request.

7. References

[1] J. Song, G. Dai, H. Zhang, J. Kong, L. Liu, Y. Li, M. Zhou, R. Gu, D. Jiang, X. Wang, Achieving 20.80% efficiency in ternary organic solar cells via suppression of static and dynamic disorder, Advanced Materials, 38 (2026) e13740.

[2] P. Murugan, Y.-L. Peng, S.-Y. Liu, H. Chen, Ternary organic solar cells: optimizing the third components, Chemical Society Reviews, 55 (2026) 5005-5038.

[3] S. Wang, L. Wang, J. Zhang, H. Gao, M. Xiao, H. Song, Third-component engineering in organic solar cells: Material innovations, morphological control, and synergistic enhancement, Nano Energy, (2025) 111329.

[4] S. Yadav, M. Pranav, C. Gangadharappa, M. Huss-Hansen, M. Schwartzkopf, J. Kjelstrup-Hansen, M. Knaapila, S. Patil, Rational third component choices drive enhanced morphology and efficiency in ternary blend organic solar cells, ACS Energy Letters, 9 (2024) 5259-5267.

[5] S. Alam, S. Sim, M.Q. Li, B.-J. Chang, J. Lee, Recent progress in semitransparent organic solar cells: photoabsorbent materials and design strategies, Micromachines, 15 (2024) 493.

[6] K. Forberich, A. Troisi, C. Liu, M. Wagner, C.J. Brabec, H.J. Egelhaaf, Guidelines for material design in semitransparent organic solar cells, Advanced Functional Materials, 34 (2024) 2314116.

[7] L. Pap, B. Schirmacher, E. Bloch, S. Bogati, P. Viehmann, A. Scheel, D. Müller, M. List, B. Zimmermann, U. Würfel, Improved light utilization efficiency for an ITO-Free semitransparent organic solar cell using a multilayer silver back electrode as infrared mirror, Solar RRL, 7 (2023) 2300561.

[8] P. Kumar, S. You, A. Vomiero, Recent progress in materials and device design for semitransparent photovoltaic technologies, Advanced Energy Materials, 13 (2023) 2301555.

[9] Z. Shokrollahi, M. Piralaee, A. Asgari, Performance and optimization study of selected 4-terminal tandem solar cells, Scientific Reports, 14 (2024) 11515.

[10] K. Liu, Y. Jiang, F. Liu, G. Ran, F. Huang, W. Wang, W. Zhang, C. Zhang, J. Hou, X. Zhu, Organic solar cells with over 19% efficiency enabled by a 2D-conjugated non-fullerene acceptor featuring favorable electronic and aggregation structures, Advanced Materials, 35 (2023) 2300363.

[11] H. Lu, W. Liu, G. Ran, Z. Liang, H. Li, N. Wei, H. Wu, Z. Ma, Y. Liu, W. Zhang, High-pressure fabrication of binary organic solar cells with high molecular weight D18 yields record 19.65% efficiency, Angewandte Chemie, 135 (2023) e202314420.

[12] Y. Zhou, W. Su, Z. Liang, Q. Wu, H. Bai, H. Liu, B. Song, X. Li, B. Xie, C. Liu, Halogenated diphenyl ether solvent additives enable∼ 20% efficiency organic solar cells and high-performance opaque/semitransparent modules, National science review, 12 (2025) nwaf346.

[13] E.A. Milani, M. Piralaee, D. Raeyani, A. Asgari, High-performance semi-transparent organic solar cells for window applications using MoO3/Ag/MoO3 transparent anodes, Solar Energy Materials and Solar Cells, 276 (2024) 113066.

[14] K. Tvingstedt, J. Benduhn, K. Vandewal, Temperature dependence of the spectral line-width of charge-transfer state emission in organic solar cells; static vs. dynamic disorder, Materials Horizons, 7 (2020) 1888-1900.